ADVANCED MATERIALS

www.advmat.de

Functionalized Porous Aromatic Frameworks as High-Performance Adsorbents for the Rapid Removal of Boric Acid from Water

*Jovan Kamcev, Mercedes K. Taylor, Dong-Myeong Shin, Nanette N. Jarenwattananon, Kristen A. Colwell, and Jeffrey R. Long**

This study demonstrates that functionalized, highly porous polymers are promising for the adsorptive capture of boric acid, a neutral contaminant that is difficult to remove from seawater using conventional reverse osmosis membranes. Appending *N*-methyl-D-glucamine (NMDG) to the pore walls of high-surface-area porous aromatic frameworks (PAFs) yields the adsorbents PAF-1-NMDG and P2-NMDG in a simple two-step synthesis. The boron-selective PAFs demonstrate adsorption capacities that are up to 70% higher than those of a commercial boron-selective resin, Amberlite IRA743, and markedly faster adsorption rates, owing to their higher NMDG loadings and greater porosities relative to the resin. Remarkably, PAF-1-NMDG is able to reduce the boron concentration in synthetic seawater from 2.91 to <0.5 ppm in less than 3 min at an adsorbent loading of only 0.3 mg mL^{-1}. The boron adsorption rate constants of both frameworks, determined via a pseudo-second-order rate model, represent the highest values reported in the literature—in most cases orders of magnitude higher than those of other boron-selective adsorbents. The frameworks can also be readily regenerated via mild acid/base treatment and maintain constant boron adsorption capacities for at least 10 regeneration cycles. These results highlight the numerous advantages of PAFs over traditional porous polymers in water treatment applications.

The global demand for clean water is increasing at a fast pace due to population growth, agricultural expansion, variable consumption patterns, climate change, and improved living standards, among other reasons.[1] As a result, freshwater resources are being depleted faster than they can replenish, creating an enormous stress on already scarce freshwater supplies.[2] Tapping into abundant, non-conventional water resources—such as seawater, municipal and industrial wastewater, and groundwater—in a sustainable and cost-effective manner will be critical for meeting these rapidly increasing water needs and ensuring water security for future generations.[3]

In this context, the capture of naturally-occurring boron—predominantly in the form of neutral boric acid—is of considerable interest, given its ubiquity in sea and groundwater, as well as in industrial and municipal wastewater.[4] Although boron is an essential micronutrient that can benefit animals and plants in low concentrations,[4b,5] excess boron can have detrimental health effects, and the permissible range for safe boron levels is often very narrow, particularly for crops and plants.[5a,6] The concentration of boron in seawater is usually between 4–6 ppm,[4a,7] but much higher values (>100 ppm) can be found in some groundwater and wastewater sources.[8] The World Health Organization has imposed a boron concentration limit of 2.4 ppm[9] for drinking water, but many countries have implemented stricter limits (<1 ppm).[4b] The boron concentration limit for irrigation water can be much lower than that for drinking water (<0.5 ppm), which poses a significant technological challenge.[4b,5a,6b]

Membrane and adsorbent-based technologies have emerged as leading water treatment strategies for highly impaired waters due to their energy efficiency, low cost, small footprint, and operational simplicity.[10] Reverse osmosis membranes currently dominate the global desalination market,[11] but state-of-the-art membranes suffer from a number of issues, including inadequate rejection of small, neutral solutes—such as boric acid at ambient conditions.[12] Indeed, single-stage reverse osmosis treatment of seawater is often unable to reduce boric acid concentrations below the strict limits set for drinking and irrigation water.[11,12b,13] As a result, removing this contaminant from water often requires additional energy-intensive steps, for example multiple reverse osmosis stages.[11] Alternative technologies for boron removal have been proposed, including adsorption, ion exchange, liquid–liquid extraction, electrodialysis, and precipitation coagulation.[4a,b,14] Among

Dr. J. Kamcev, Dr. M. K. Taylor, Dr. D.-M. Shin,
Dr. N. N. Jarenwattananon, Dr. K. A. Colwell, Prof. J. R. Long
Department of Chemistry
University of California, Berkeley
Berkeley, CA 94720, USA
E-mail: jrlong@berkeley.edu

Dr. J. Kamcev, Dr. M. K. Taylor, Prof. J. R. Long
Materials Sciences Division
Lawrence Berkeley National Laboratory
Berkeley, CA 94720, USA

Dr. K. A. Colwell, Prof. J. R. Long
Department of Chemical and Biomolecular Engineering
University of California, Berkeley
Berkeley, CA 94720, USA

The ORCID identification number(s) for the author(s) of this article can be found under https://doi.org/10.1002/adma.201808027.

DOI: 10.1002/adma.201808027

these alternatives, adsorption has emerged as the most promising technology due to its low cost, excellent selectivity, and operational simplicity.[15]

Adsorption-based technologies for boron removal from aqueous solutions primarily rely on boron-selective resins, which are typically made from polymers bearing boron chelating moieties (e.g., polyol groups).[4c,15] Other materials have also been explored for boron adsorption, including activated carbons and metal oxides, but their performance is often inferior to that of polymeric resins because they typically lack the boron-specific polyol functional groups.[15] High-performance adsorbents must possess—at a minimum—excellent selectivity, large capacities, fast adsorption rates, long-term stability, and reusability. However, most boron-selective adsorbents fall short in at least one of these areas, thereby severely limiting their effectiveness for water treatment applications.

Porous aromatic frameworks (PAFs) are a relatively new class of porous network polymers with desirable properties including exceptionally high surface areas (>5600 m^2 g^{-1}), remarkable long-term stability in harsh environments, and chemical structures that are amenable to modification with a diverse array of functionalities.[16] These properties render PAFs promising for use as adsorbents in water treatment applications. While PAFs have been extensively investigated as adsorbents for gas storage and separation applications,[17] their utility in water treatment applications, and boron capture in particular, remains relatively unexplored.[18] Herein, we demonstrate that PAFs can provide an excellent platform for the development of high-performance adsorbents for water treatment applications. In particular, modification of two high-surface-area porous polymers, PAF-1 and P2, via functionalization with *N*-methyl-D-glucamine (NMDG) yields adsorbents that exhibit exceptional selectivity for boron and rapid adsorption relative to a state-of-the art commercial resin, Amberlite IRA743. Remarkably, these materials exhibit adsorption kinetics that far exceed those of any boron-selective material reported to date, highlighting the potentially significant energy savings that may be accessed by using PAFs in the treatment of water for the removal of boron and other contaminants.

The parent frameworks PAF-1[16a] and P2[19] were synthesized from tetrakis(4-bromophenyl)methane via a Yamamoto-type Ullmann coupling reaction and a Suzuki cross-coupling reaction between tetrakis(4-bromophenyl)methane and 1,4-benzenediboronic acid bis(pinacol) ester, respectively. Successful synthesis of both materials was confirmed by data from Fourier transform infrared spectroscopy (FTIR), elemental analysis, and solid state ^{1}H–^{13}C cross-polarization magic angle spinning (MAS) nuclear magnetic resonance (NMR) spectroscopy (see Section 2 in the Supporting Information), which agreed with previously published results.[16a,19]

The boron-selective PAFs were synthesized via a two-step post-synthetic modification of PAF-1 and P2, as illustrated in **Figure 1**. In the first step, PAF-1 and P2 were chloromethylated

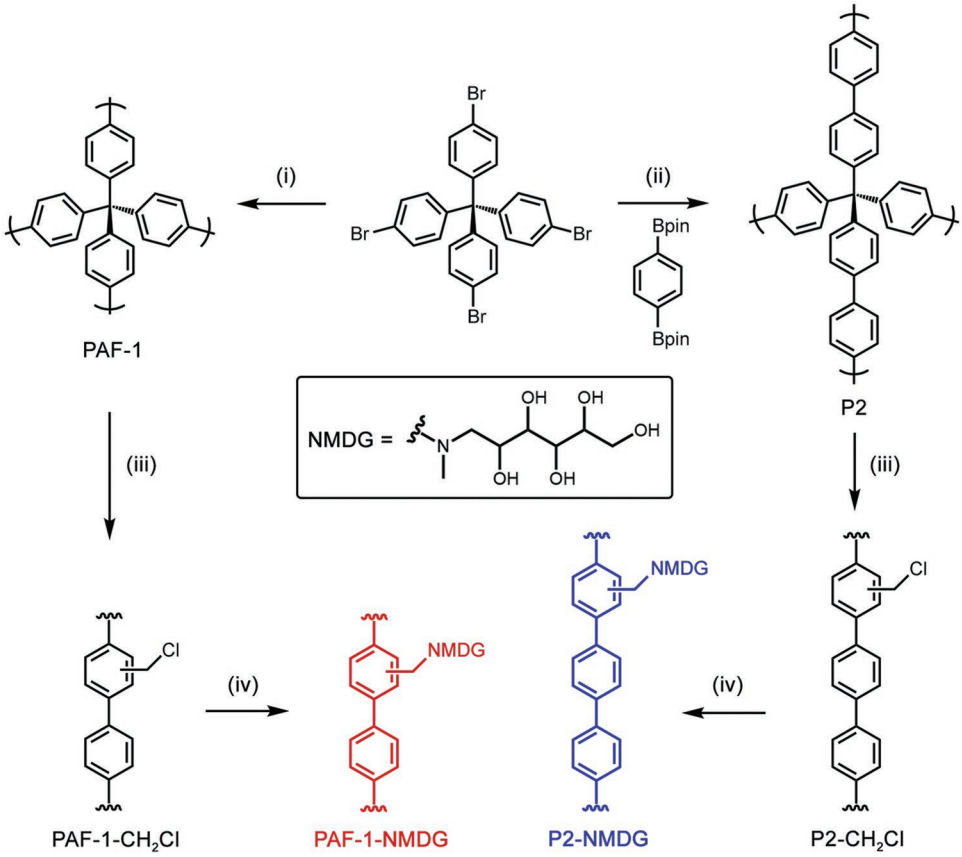

Figure 1. General scheme for the synthesis of boron-selective adsorbents PAF-1-NMDG and P2-NMDG. Reaction conditions: i) $Ni(cod)_2$, cod, 2,2′-bipyridine, *N*,*N*-dimethylformamide, 80 °C; ii) XPhos Pd G2, THF, 65 °C; iii) paraformaldehyde, AcOH, H_3PO_4, HCl, 90 °C; and iv) NMDG, *N*,*N*-dimethylformamide, 90 °C.

according to a previously reported protocol to access PAF-1-CH_2Cl and P2-CH_2Cl.[17d] The successful introduction of –CH_2Cl moieties into each framework was confirmed by the appearance of an absorption band around 1266 cm^{-1} in their FTIR spectra, attributed to the methylene wagging mode of –CH_2Cl, and via MAS ^{13}C NMR spectroscopy by the appearance of a new resonance at 43 ppm. Based on carbon elemental analysis, chloromethylation yielded approximately 1.18 and 1.62 –CH_2Cl groups per biphenyl and terphenyl for PAF-1-CH_2Cl and P2-CH_2Cl, respectively.

In the second modification step, NMDG was appended to the pore walls of the frameworks via a nucleophilic substitution reaction with the –CH_2Cl groups. Successful incorporation of NMDG was confirmed via FTIR spectroscopy, with the disappearance of the band at 1266 cm^{-1} and the appearance of three new bands at 1072, 1017, and 3300–3600 (broad) cm^{-1} that were attributed to the C–O, C–N, and hydroxyl groups of NMDG, respectively.[20] Further support for successful incorporation of NMDG was afforded from MAS ^{13}C NMR spectroscopy, with the appearance of a broad resonance at ≈72 ppm that was attributed to the carbon atoms in NMDG. Based on nitrogen elemental analysis data, the overall reaction yielded approximately 0.87 and 1.07 NMDG functional groups per biphenyl and terphenyl for PAF-1-NMDG and P2-NMDG, respectively (corresponding to NMDG loadings of 2.55 and 2.33 mmol g^{-1}, respectively). Calculations from carbon elemental analysis data yielded similar values (see the Supporting Information for details).

Nitrogen adsorption isotherms collected at 77 K were used to quantify the surface areas of the parent frameworks and their functionalized analogs (Figure S3, Supporting Information). The Brunauer–Emmett–Teller (BET) surface areas of PAF-1 and P2 were determined to be 4400 and 1550 m^2 g^{-1}, respectively. The lower surface area of P2—despite its longer repeat unit—is attributed to network interpenetration during framework assembly,[17a] as well as the presence of unreacted aryl bromide end groups that contribute to the total framework mass.[16c] In contrast, PAF-1 is considered to be a non-interpenetrating framework with no residual aryl bromide end groups remaining on the framework surface following synthesis.[16c] As expected, appending –CH_2Cl groups to PAF-1 and P2 reduced their surface areas to 1960 and 1200 m^2 g^{-1}, respectively. Following the reaction to append the rather bulky NMDG functional groups, the final surface areas of PAF-1-NMDG and P2-NMDG were determined to be 78.8 and 28.6 m^2 g^{-1}, respectively.

Upon successful synthesis of PAF-1-NMDG and P2-NMDG, we investigated their equilibrium boron uptake via batch adsorption experiments and compared their performance with that of a leading commercial boron-selective polymeric resin, Amberlite IRA743. The commercial resin is made from NMDG-functionalized poly(styrene-divinylbenzene),[4b] and elemental analysis of a sample obtained from Sigma–Aldrich (Amberlite IRA743 free base) indicated an NMDG loading of 2.18 mmol g^{-1}, assuming all of the detected nitrogen content was due to the NMDG functional groups. The BET surface area of the IRA743 resin was 23.4 m^2 g^{-1} (Figure S6, Supporting Information), which is in reasonable agreement with previous reports.[21] Equilibrium boron adsorption capacities as a function of equilibrium boron concentration in the contiguous solution are presented in **Figure 2**a. Both PAF-1-NMDG and P2-NMDG demonstrated higher boron adsorption capacities than IRA743. On average, PAF-1-NMDG also exhibited slightly higher boron adsorption than P2-NMDG, which is reasonable given the higher surface area of PAF-1-NMDG and its higher density of NMDG groups compared to P2-NMDG.

The equilibrium adsorption data were fit using a single-site Langmuir model, which provided a reasonably good description of the experimental results (see section 6 in the Supporting Information for full details). The saturation capacities of PAF-1-NMDG and P2-NMDG were determined to be 1.70 and 1.56 mmol g^{-1}, respectively—approximately 70% and 56% higher than that determined for IRA743 (0.991 mmol g^{-1}).[22] Given that the Langmuir model slightly underestimates boron adsorption by both PAFs at higher concentrations, their actual saturation capacities are likely to be slightly larger than predicted

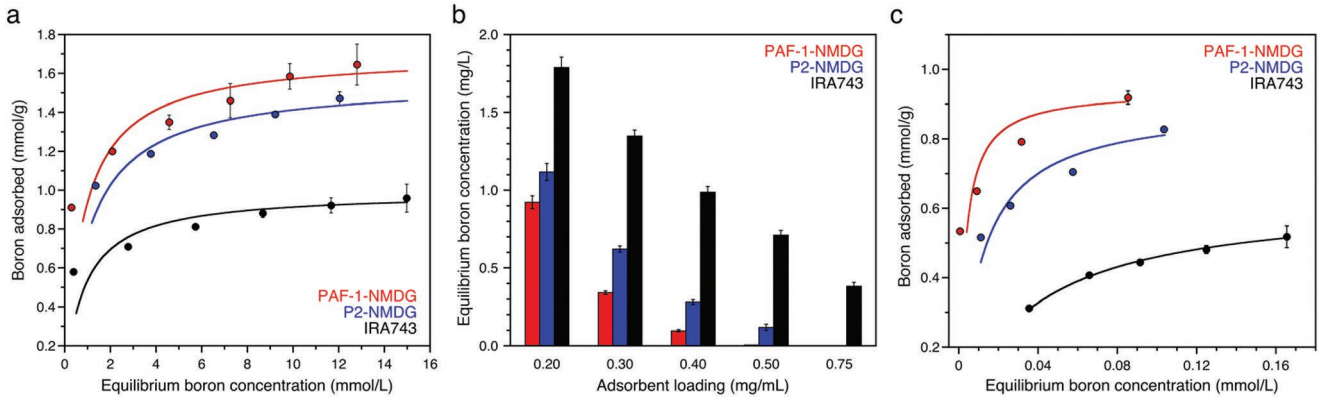

Figure 2. a) Equilibrium boron adsorption capacity as a function of equilibrium boron concentration in aqueous boric acid solutions prepared with DI water (initial concentrations ranging from 1.6 to 19.4 mmol L^{-1}). b) Equilibrium boron concentrations in synthetic seawater (initial boron concentration of 2.91 mg L^{-1}, pH of 8.2) as a function of adsorbent loading. c) Boron adsorption capacities as a function of equilibrium boron concentration in synthetic seawater. Error bars represent the standard deviation obtained from measurements on at least three separate samples. Filled symbols in (a) and (c) denote experimental points and solid lines represent Langmuir model fits. Langmuir model parameters and R^2 values are provided in section 6 of the Supporting Information.

here. Notably, PAF-1-NMDG and P2-NMDG also exhibit high saturation capacities relative to other polymeric boron-selective adsorbents (see Table S4, Supporting Information). Recently, some inorganic materials such as nitrogen-doped graphene oxide[23] and metal–organic frameworks[24] have also been shown to exhibit impressive boron capacities—as high as 10.6 mmol g^{-1} (at 45 °C) for the metal–organic framework UiO-66. However, these materials undergo significant reductions in boron adsorption capacity after a few regeneration cycles, casting doubt on their long-term performance.

Selective removal of boron from aqueous solutions in the presence of other solutes is important for practical applications, such as seawater desalination. In practice, boron-selective adsorbents are likely to be used after passing seawater through a single stage of reverse osmosis, after which the concentration of competing ions is substantially lowered. In this study, however, the selectivity of the NMDG-functionalized PAFs was tested in solutions mimicking untreated seawater, representing some of the most challenging boron-removal conditions likely to be encountered. The measured concentration of boron in the synthetic seawater solution was 2.91 ppm (or 16.4 ppm boric acid), and the concentrations of all other ions (Na^+, K^+, Mg^{2+}, Ca^{2+}, Sr^{2+}, Cl^-, HCO_3^-, SO_4^{2-}, Br^-, and F^-) ranged from 1.36 mg L^{-1} to ≈19.8 g L^{-1}, as reported by the manufacturer (see Table S5, Supporting Information). For these experiments, the adsorbent concentration varied from 0.20 to 0.75 mg mL^{-1}.

For all adsorbent quantities investigated, the PAFs removed a larger amount of boron from the synthetic seawater samples than IRA743 (Figure 2b). In particular, while a maximum ≈86% reduction in initial boron concentration was achieved with the highest IRA743 loading of 0.75 mg mL^{-1}, PAF-1-NMDG and P2-NMDG loadings of 0.5 and 0.75 mg mL^{-1}, respectively, reduced boron levels below those detectable by ICP-OES. Approximately 0.3 and 0.4 mg of PAF-1-NMDG and P2-NMDG per mL of synthetic seawater, respectively, were required to reduce the boron concentration to below 0.5 ppm, which is a common target for irrigation water. In contrast, ≈0.75 mg L^{-1} of IRA743 was required to reach this target. These results demonstrate that the NMDG-functionalized PAFs are able to efficiently remove boron at low adsorbent concentrations from aqueous solutions containing highly concentrated ionic species commonly found in seawater.

Boron adsorption capacities as a function of equilibrium boron concentration in synthetic seawater solutions are presented in Figure 2c. A Langmuir model was again used to fit the data and extract boron saturation capacities of 0.94, 0.90, and 0.63 mmol g^{-1} for PAF-1-NMDG, P2-NMDG, and IRA743, respectively—a trend that mirrored the non-competitive adsorption experiments. These saturation adsorption capacities are ≈40% lower than those obtained in boric acid solution, suggesting that the other ionic species in the synthetic seawater interfere with the complexation process. Competitive adsorption studies reported for other boron-selective polymers have also revealed a reduction in boron adsorption in the presence of various ions.[25]

Interestingly, under competitive adsorption conditions, both PAFs outperformed other boron-selective materials that demonstrate better performance under non-competitive conditions. For example, the saturation capacity of nitrogen-doped graphene oxide was found to be 5.43 mmol g^{-1} in boric acid solution, compared to values of 1.70 and 1.56 mmol g^{-1} for PAF-1-NMDG and P2-NMDG, respectively, under similar experimental conditions.[23] However, in synthetic seawater the nitrogen-doped graphene oxide capacity diminished to 0.23 mmol g^{-1}, compared to 0.94 and 0.90 mmol g^{-1} for PAF-1-NMDG and P2-NMDG, respectively.

The complexation of NMDG and boron species can result in a number of different structures, and the type of complex formed directly influences the boron adsorption capacity of a material. For example, one NMDG group can form either a monochelate or a tetradentate complex with one borate, or two NMDG groups can form a bischelate complex with one borate (**Figure 3**a).[26] Excluding other criteria, the adsorption capacity of a material that forms monochelate or tetradentate complexes would be higher than the material that forms bischelate complexes. To elucidate the nature of the complexation that occurs within PAF-1-NMDG and P2-NMDG, boron-saturated samples of both materials were characterized via ^{11}B MAS NMR and FTIR spectroscopy (Figure 3b,c).

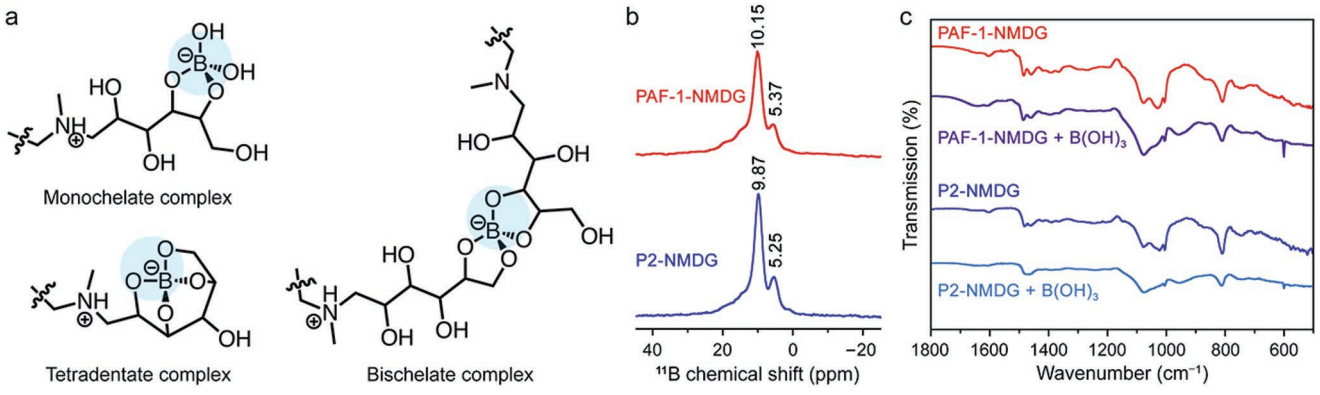

Figure 3. a) Possible NMDG-borate complex structures. b) ^{11}B MAS NMR and spectra of PAF-1-NMDG and P2-NMDG after exposure to 2000 ppm aqueous boric acid solution. Two well-resolved peaks were observed in each spectrum, with chemical shifts of 10.15 and 5.37 ppm for PAF-1-NMDG and 9.87 and 5.25 ppm for P2-NMDG. c) FTIR spectra of PAF-1-NMDG (red), P2-NMDG (blue), and PAF-1-NMDG and P2-NMDG following exposure to a 2000 ppm aqueous boric acid solution (purple and pale blue, respectively).

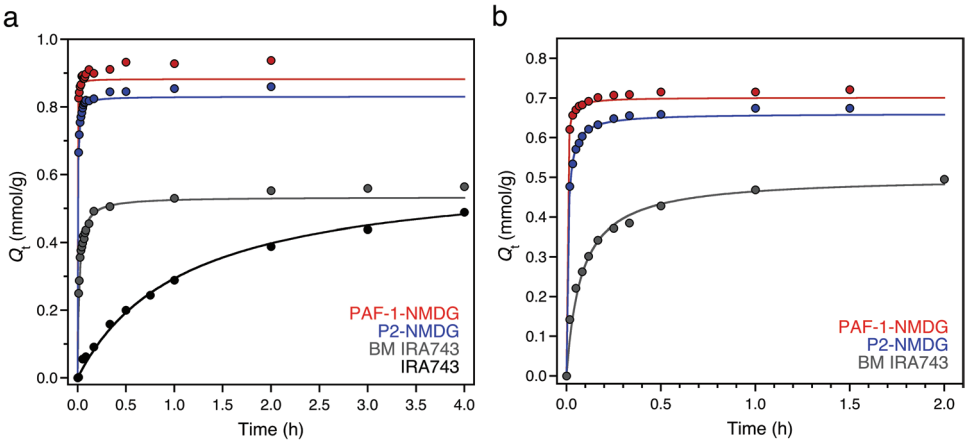

Figure 4. a) Time-dependent boron (as boric acid) adsorption capacities, Q_t, of PAF-1-NMDG, P2-NMDG, IRA743, and BM IRA743. The solution loading of each adsorbent was 1 mg mL^{-1} and the initial boric acid concentration was 80 ppm (1.29 mmol L^{-1}). b) Time-dependent boron (as boric acid in synthetic seawater) adsorption capacities, Q_t, of PAF-1-NMDG, P2-NMDG, and BM IRA743. The solution loading of each adsorbent was 0.3 mg mL^{-1} and the initial boron concentration was 2.91 ppm.

Exposure of PAF-1-NMDG and P2-NMDG to a 2000 ppm boric acid solution resulted in the appearance of a peak at ≈950 cm^{-1} in their IR spectra, which was attributed to the asymmetric B—O stretch of the tetrahedral borate anion.[27] The absence of a peak at ≈1400 cm^{-1}, corresponding to the asymmetric B—O stretch of trigonal boric acid, suggests that nearly all of the complexed boron was in the form of tetrahedral borate. The ^{11}B MAS NMR spectra of both PAFs exhibited two distinct chemical shifts at approximately 5 and 10 ppm (Figure 3c), consistent with the previously reported ^{11}B MAS NMR spectra for IRA743.[22] We attributed the chemical shifts at ≈5 ppm to monochelate NMDG–borate complexes, while the chemical shifts at ≈10 ppm were assigned to either bischelate or tetradentate complexes, based on previous assignments of the IRA743 spectrum.[22,26] Considering the density of NMDG sites in all three materials, the maximum boron capacities are lower than would be expected for one-to-one NMDG–borate complex formation (e.g., 2.4 mmol g^{-1} in the case of PAF-1-NMDG, assuming all NMDG groups are accessible), but they are also higher than expected for exclusive formation of bischelate complexes (e.g., 1.2 mmol g^{-1} in the case of PAF-1-NMDG). Thus, we attributed the chemical shifts at ≈10 ppm to a mixture of both the bischelate and tetradentate complexes. Based on the relative intensities of the two chemical shifts for both PAFs, the formation of bischelate and tetradentate complexes is favored over the formation of monochelate species.

The rate of solute adsorption within a material is a key property that determines industrial batch processing times. The rate of boron adsorption within the PAFs and IRA743 was investigated via batch adsorption experiments, using aqueous solutions consisting of 80 ppm boric acid and adsorbent quantities of 1 mg mL^{-1} of solution. Interestingly, it was found that the boron adsorption rate for PAF-1-NMDG determined using initially dry samples differed substantially from the rate measured using samples initially equilibrated with water (see Figure S10, Supporting Information). The discrepancy may be attributed to rate-limiting water diffusion through the pores and accompanying particle agglomeration in the dry material, which would be minimized in a hydrated, well-dispersed sample. Thus, prior to boron exposure all adsorbents were equilibrated with a small amount of deionized (DI) water.

As shown in **Figure 4**a, both PAFs achieved their equilibrium boron adsorption capacities significantly faster than IRA743 (see Figure S11, Supporting Information for time-dependent boron adsorption data normalized by the equilibrium adsorption capacity for each material). This result was somewhat expected due to the substantially smaller PAF particle sizes—on the order of hundreds of nm (Figure S5, Supporting Information) relative to 500–700 µm for the resin. To minimize any size effects, a sample of IRA743 was ball-milled (BM) for 30 min at a frequency of 30 Hz to yield average particle sizes comparable to that of the PAFs (Figure S5, Supporting Information). Kinetics experiments performed under the same conditions revealed more rapid boron adsorption by the BM IRA743 sample, but this rate was still surpassed by that of both PAFs—for example, after 30 s, PAF-1-NMDG and P2-NMDG reached ≈90% and ≈78% of their equilibrium capacities, respectively, while BM IRA743 achieved less than 50% of its equilibrium capacity.

A linearized pseudo-second-order rate model, given by equation (1),[28] was used to analyze the boron adsorption rates for each material.

$$\frac{t}{Q_t} = \frac{1}{\left(k_2 Q_e^2\right)} + \frac{t}{Q_e} \quad (1)$$

Here, Q_t is the boron adsorption capacity at time t (units of mg g^{-1}), Q_e is the boron adsorption capacity at equilibrium (units of mg g^{-1}), and k_2 is the rate constant (units of g mg^{-1} h^{-1}). The data points in the transient region of each plot ($Q_t/Q_e < 0.95$) were fitted to equation (1) to extract Q_e and k_2 (see **Table 1**), and the fits are presented in Figure 4a as solid lines. Overall, the pseudo-second-order rate model provided a reasonably good description of the experimental results, in agreement with previous reports on boron adsorption in polymeric materials (see Table S6, Supporting Information). The lowest pseudo-second-order rate constant was observed for IRA743, due to its much larger particle size relative to the other adsorbents as mentioned above. BM increased the pseudo-second-order rate constant of

Table 1. Pseudo-second-order rate model parameters for experiments performed with boric acid (80 ppm) or synthetic seawater solutions. All experimental data were fit with $R^2 > 0.99$. Equilibrium adsorption capacities, Q_e, are given in units of mg (boron) g^{-1} and k_2 values are given in units of g mg^{-1} h^{-1}.

Adsorbent	Boric acid solution		Synthetic seawater	
	Q_e	k_2	Q_e	k_2
PAF-1-NMDG	9.54	164	7.58	59.9
P2-NMDG	8.98	46.5	7.14	18.6
IRA743	6.64	0.138	–	–
BM IRA743	5.77	10.4	5.42	2.32

IRA743 by a factor of ≈75, and such a strong rate dependence on particle size suggests that diffusion of boric acid within the pores is the rate limiting step in adsorption. Both PAFs demonstrated substantially faster rates of boron adsorption relative to the commercial resin—for example, the rate constants for PAF-1-NMDG and P2-NMDG were 16 and 4.5 times greater than that of BM IRA743, respectively. To the best of our knowledge, the pseudo-second-order rate constants for the PAFs represent the highest values reported to date for any boron-selective material, regardless of experimental conditions. For comparison, an extensive list of rate constants for boron adsorption in various adsorbents is provided in the Supporting Information (see Table S6).

The remarkably high rate of boron adsorption demonstrated by PAF-1-NMDG can be primarily attributed to its greater porosity relative to that of the other materials, as indicated by its larger BET surface area. Interestingly, P2-NMDG and BM IRA743 possess comparable BET surface areas, but the rate constant for P2-NMDG is more than four times that of BM IRA743. This result could arise if the particle sizes between the two materials remained somewhat disparate even after BM—although this conclusion is difficult to draw with certainty from the scanning electron microscopy (SEM) images alone, because particle agglomeration during imaging made it difficult to precisely determine average particle size. The faster boron adsorption by P2-NMDG relative to that of BM IRA743 might also be partly attributed to swelling of the framework in the presence of water, which would enhance its porosity and internal pore volume available for mass transfer. Indeed, previous studies have suggested that similar porous network polymers may be susceptible to swelling,[29] which could be undetectable via standard surface area measurements—especially for materials possessing chemical functionalities that interact strongly (e.g., via hydrogen bonding) and do not allow the framework to easily expand in the presence of gases.[29]

To investigate whether the porosities of PAF-1-NMDG and P2-NMDG are substantially different in the presence of water, we performed water vapor isotherm measurements at 25 °C (Figure S12, Supporting Information). Interestingly, water adsorption in P2-NMDG was greater than that in BM IRA743 despite the similar nitrogen adsorption in these two materials, indicating that P2-NMDG may indeed swell to some extent in the presence of water. This result suggests that water-equilibrated P2-NMDG exhibits greater porosity and pore volume available for mass transfer than water-equilibrated BM IRA743, which would account for the faster rate of boron adsorption exhibited by P2-NMDG. Water vapor adsorption was the highest in PAF-1-NMDG, indicating that the hydrated material has greater porosity than both P2-NMDG and IRA743, which is also corroborated by the N_2 surface area and boron adsorption kinetics results. However, further investigation is necessary to fully understand this behavior.

Rate experiments were also performed with a synthetic seawater solution to test the performance of the materials under competitive adsorption conditions. In general, the trends observed for the non-competitive experiments were preserved—PAF-1-NMDG exhibited the highest rate of boron adsorption, followed by P2-NMDG and then BM IRA743 (Figure 4b). Within 1 min, PAF-1-NMDG and P2-NMDG achieved 86% and 71% of their equilibrium adsorption capacities, respectively, while BM IRA743 reached only 28% of its equilibrium capacity. Notably, PAF-1-NMDG reduced the concentration of boron in the synthetic seawater solution from 2.91 to less than 0.5 ppm in just 3 min. This is a remarkable result considering the low adsorbent concentration employed for these experiments, as well as the high concentration of various other ionic species in the synthetic seawater.

Boron adsorption rate constants were again determined by fitting data in the transient region ($Q_t/Q_e < 0.95$) to the linearized pseudo-second-order rate model in equation (1) (Table 1 and solid lines in Figure 4b). The rate constant for PAF-1-NMDG was determined to be 59.9 g mg^{-1} h^{-1}, approximately 26 times higher than the rate constant for BM IRA743 and three times higher than that of P2-NMDG. For all materials, the pseudo-second-order rate constants derived from the competitive adsorption experiments were lower than those from the non-competitive adsorption experiments. This result was expected, since the boron concentration in the synthetic seawater solution was lower than that in the pure boric acid solution, thereby lowering the driving force for boron diffusion within the materials. Nevertheless, the pseudo-second-order rate constants for both PAFs under these challenging competitive conditions remain higher than all other values reported in the literature for boron-selective adsorbents under any experimental conditions (Table S6, Supporting Information).

The ability to fully regenerate and reuse adsorbents over many cycles is critical for their practical implementation and may justify initially high material costs. In the case of the NMDG–borate complex, exposure to an acidic solution can lead to a release of boric acid[4c] and subsequent treatment with base will regenerate the neutral NDMG tertiary amine. We thus evaluated the cyclability of PAF-1-NMDG and P2-NMDG by first treating each adsorbent (5 mg mL^{-1}) with a 400 ppm of boric acid solution, washing each material with 1 M HCl followed by 1 M NaOH, and finally re-exposing each to fresh boric acid solution. Notably, both PAFs maintained their boron adsorption capacities for at least 10 of these cycles (**Figure 5**), demonstrating their excellent stability and reusability.

Due to their high porosities, excellent stability, and ease of functionalization, PAFs are emerging as promising high-performance adsorbents for water treatment applications. We have leveraged the tunability of these materials to design two novel boron-selective adsorbents by appending NMDG functional groups to the pore walls of the frameworks PAF-1 and P2

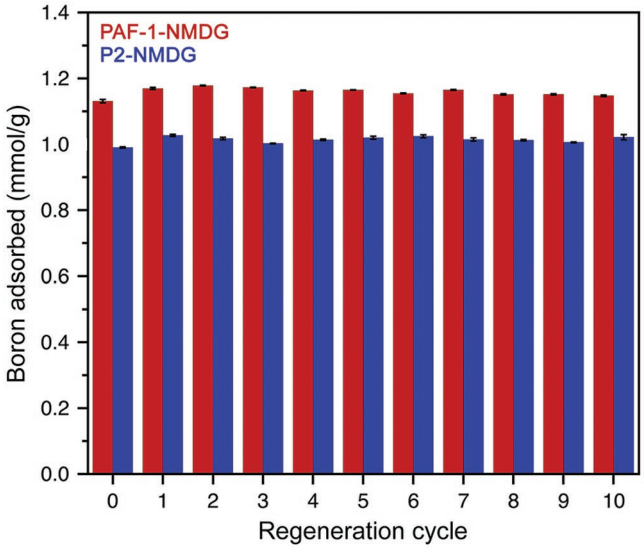

Figure 5. Boron adsorption as a function of regeneration cycle number. The solution loading of each adsorbent was 5 mg mL^{-1}, and the boric acid concentration in the external solution was 400 ppm (6.47 mmol L^{-1}).

via a facile two-step reaction. The resulting PAF-1-NMDG and P2-NMDG materials demonstrate boron capacities that are as much as 70% greater than that of the commercial resin IRA743 under non-competitive and competitive conditions. Additionally, relative to the resin, significantly smaller amounts of each PAF were required to reduce the boron concentration in synthetic seawater to below 0.5 ppm, a common target concentration for irrigation water. To the best of our knowledge the boron adsorption rate constants of PAF-1-NMDG and P2-NMDG in both boric acid and synthetic seawater solutions represent the highest values reported in the open literature for any boron-selective adsorbent. Importantly, both PAFs could also be regenerated via mild acid/base treatment and maintained their initial boron capacities for at least 10 regeneration cycles. These results demonstrate the promise of using functionalized PAFs as high-performance adsorbents for difficult water treatment applications.

Experimental Section

Materials: Tetrakis(4-bromophenyl)methane was synthesized according to a previously reported procedure.[30] All other starting materials and reagents were purchased from Sigma–Aldrich and used as received, unless otherwise stated.

PAF-1 Synthesis: A three-neck Schlenk flask was charged with bis(1,5-cyclooctadiene)nickel(0) (2.0 g, 7.3 mmol), dried 2,2′-bipyridyl (1.1 g, 7.3 mmol), anhydrous dimethylformamide (DMF) (110 mL), and 1,5-cyclooctadiene (0.93 mL) under an argon atmosphere. The mixture was heated to 80 °C and stirred for 1 h to afford a deep purple solution. Dried tetrakis(4-bromophenyl)methane (0.93 g, 1.5 mmol) was added to the flask under an argon atmosphere via a solid transfer adapter, and the mixture was stirred overnight at 80 °C, after which the solution had changed color to black. Upon cooling to room temperature, aqueous 6 M hydrochloric acid (50 mL) was added dropwise to the flask, and the resulting turquoise solution was stirred for 3 h at room temperature. After stirring for ≈30 min, the color of the initially black particles changed to white. The white solid was filtered and washed with DMF (250 mL), methanol (250 mL), chloroform (250 mL), methylenedichloride (250 mL), and tetrahydrofuran (THF, 250 mL), and dried under vacuum at 150 °C to afford ≈440 mg of PAF-1 as an off-white powder.

P2 Synthesis: A 150 mL Schlenk flask was charged with tetrakis(4-bromophenyl)methane (500 mg, 0.79 mmol), 1,4-benzenediboronic acid bis(pinacol) ester (540 mg, 1.7 mmol), and chloro(2-dicyclohexylphosphino-2′,6′-dimethoxy-1,1′-biphenyl)[2-(2′-amino-1,1′-biphenyl)]palladium(II) (SPhos Pd G2) (55 mg, 0.076 mmol). The solid mixture was then deoxygenated with three vacuum/argon cycles. Anhydrous THF (25 mL) and degassed aqueous 2 M K_2CO_3 (2.5 mL) were then added to the flask via syringe transfer under an argon atmosphere. The solution was stirred at 65 °C for 3 d, during which a white precipitate appeared. The solid was filtered, washed with THF (250 mL), and then stirred in aqueous 6 M HCl (50 mL) for ≈6 h to remove impurities and side products. The solid was then collected via vacuum filtration and washed with 250 mL each of THF, methanol, and methylene dichloride. The solid was further purified via Soxhlet extraction with THF and methylene dichloride (24 h each). The product was then dried under vacuum at 150 °C to afford ≈350 mg of P2 as a beige powder.

PAF-1-CH_2Cl and P2-CH_2Cl Synthesis: A 150-mL pressure vessel was charged with either PAF-1 or P2 (300 mg), paraformaldehyde (1.5 g, 0.050 mol as monomer), glacial acetic acid (9.0 mL, 0.16 mol), phosphoric acid (4.5 mL, 0.086 mol), and 12.1 M hydrochloric acid (30 mL, 0.36 mol). The mixture was stirred at 90 °C for 3 d. The solid was filtered, washed with methanol (1.0 L), and dried under vacuum at 120 °C overnight to afford PAF-1-CH_2Cl (≈400 mg) or P2-CH_2Cl (≈360 mg) as a beige powder.

PAF-1-NMDG and P2-NMDG Synthesis: A 150-mL pressure vessel was charged with either PAF-1-CH_2Cl or P2-CH_2Cl (300 mg), NMDG (12 g, 0.061 mol), and DMF (40 g). The mixture was stirred at 90 °C for 3 d. After this time, the solid was filtered, washed with methanol (1.5 L), and dried under vacuum at 120 °C overnight to afford PAF-1-NMDG (≈460 mg) or P2-NMDG (≈430 mg) as a light beige powder. Prior to all measurements, the frameworks were dried under vacuum at 120 °C overnight to remove any residual solvent.

Equilibrium Boron Adsorption: After drying, a sample of PAF-1-NMDG, P2-NMDG, or IRA743 (≈10 mg) was quickly weighed in a plastic 4-mL tube using a microbalance (XPE Micro-analytical Balance, Mettler Toledo, Columbus, OH, USA). Then, an aqueous boric acid solution (≈2 mL, 100–1200 ppm) prepared with ultrapure DI water (or synthetic seawater solution for the competitive adsorption experiments) was added to the plastic vial, and the mixture was shaken for 24 h at 25 °C. Ultrapure DI water (18.2 MΩ cm electrical resistivity and less than 5.4 ppb total organic carbon) was generated by a Millipore RiOS and A10 water purification system (Billerica, MA, USA). After equilibration, the solution was filtered through a 0.45 µm syringe filter to remove the particles, and the concentration of boron in the solution was quantified via inductively coupled plasma optical emission spectrometry (ICP-OES, Optima 7000 DV, PerkinElmer, Weltham, MA, USA). The boron adsorption capacity, Q_e (mmol g^{-1}), was calculated from the following equation:

$$Q_e = (C_0 - C_e)V\,m^{-1} \quad (2)$$

where C_0 is the initial boron concentration in the solution (mmol L^{-1}), C_e is the boron concentration in the solution after equilibration (mmol L^{-1}), V is the solution volume (L), and m is the adsorbent mass (g). A similar protocol was used to measure equilibrium boron adsorption as a function of solution pH. The solution pH was adjusted with aqueous HCl or NaOH.

Boron Adsorption Kinetics: After drying, a sample of PAF-1-NMDG, P2-NMDG, or IRA743 (≈30 mg) was quickly weighed and added to a 50-mL plastic centrifuge tube containing a magnetic stir bar. The centrifuge tube was then charged with 6 mL of DI water, and the solution was stirred at 1000 rpm for ≈1 h to disperse and hydrate the adsorbent. An aqueous solution of boric acid prepared in DI water (24 mL, 100 ppm) was then added to the centrifuge tube to reach a final desired boric acid concentration (80 ppm), and the solution was stirred

at 1300 rpm at ambient conditions. For the competitive adsorption experiments, the powder samples (≈12 mg) were equilibrated with 1 mL of DI water prior to adding 39 mL of synthetic seawater solution. At fixed time intervals, 500-µL aliquots of the solution were collected and quickly filtered with a 0.45-µm syringe filter. The concentration of boron in the solution was measured via ICP-OES, and the amount of boron adsorbed in the material was calculated via equation (2).

Adsorbent Regeneration: After drying, PAF-1-NMDG or P2-NMDG (typically 200 mg) was quickly weighed and added to a 50-mL plastic centrifuge tube containing a magnetic stir bar. Then, a 400 ppm aqueous boric acid solution (40 mL) was added to the tube, and the mixture was stirred at 1300 rpm for ≈2 h. After equilibration, the adsorbent was filtered and washed sequentially with 150 mL each of DI water, 1 M HCl, DI water, 1 M NaOH, DI water, and methanol and subsequently dried under vacuum. After drying, the mass of the adsorbent was recorded and the experimental protocol was repeated.

^{11}B NMR Spectroscopy: ^{11}B solid-state MAS NMR spectra were acquired at room temperature using a Bruker AV-500 spectrometer equipped with a 4 mm 1H/X MAS probe (Bruker). A MAS frequency of 10 kHz was used for all ^{11}B signal acquisitions. Spectra were acquired using a Hahn-echo pulse sequence with a 90° pulse of 6 µs and a recycle delay of 5 s. Interpulse spacings were rotor synchronized to 300 µs to minimize the boron nitride background signal of the MAS stator. Acquisition with shorter interpulse spacings (100–200 µs) did not demonstrate additional boron peaks, aside increased signal from the stator background. The ^{11}B chemical shifts were calibrated using 0.1 M boric acid aqueous solution as an external reference.

Supporting Information

Supporting Information is available from the Wiley Online Library or from the author.

Acknowledgements

The synthesis and characterization of PAF-1 and P2 were supported by the Center for Gas Separations, an Energy Frontier Research Center funded by the U.S. Department of Energy, Office of Science, Office of Basic Energy Sciences, under Award DE-SC0001015. All other aspects of this research were supported by the Laboratory Directed Research and Development Program of Lawrence Berkeley National Laboratory under U. S. Department of Energy Contract DE-AC02-05CH11231. The authors thank personnel within the College of Chemistry NMR facility for assistance with MAS NMR experiments and personnel within the California Institute for Quantitative Biosciences for assistance with SEM energy-dispersive spectroscopy (EDS) analysis. Additionally, the authors would like to acknowledge the National Science Foundation for graduate fellowship support of M.K.T., and Dr. Katie R. Meihaus of the University of California, Berkeley for editorial assistance.

Conflict of Interest

The authors declare no conflict of interest.

Keywords

adsorption, boron-selective adsorbents, porous aromatic frameworks, water purification

Received: December 12, 2018
Revised: February 17, 2019
Published online: March 18, 2019

[1] a) M. A. Hanjra, M. E. Qureshi, *Food Policy* **2010**, *35*, 365; b) M. M. Mekonnen, A. Y. Hoekstra, *Sci. Adv.* **2016**, *2*, e1500323; c) C. J. Vorosmarty, P. Green, J. Salisbury, R. B. Lammers, *Science* **2000**, *289*, 284.
[2] a) P. H. Gleick, *Science* **2003**, *302*, 1524; b) A. Y. Hoekstra, M. M. Mekonnen, A. K. Chapagain, R. E. Mathews, B. D. Richter, *PLoS One* **2012**, *7*, e32688.
[3] a) P. Gikas, A. N. Angelakis, *Desalination* **2009**, *248*, 1049; b) M. Qadir, B. R. Sharma, A. Bruggeman, R. Choukr-Allah, F. Karajeh, *Agric. Water Manage.* **2007**, *87*, 2; c) M. A. Shannon, P. W. Bohn, M. Elimelech, J. G. Georgiadis, B. J. Marinas, A. M. Mayes, *Nature* **2008**, *452*, 301; d) G. M. von Medeazza, *Desalination* **2004**, *169*, 287.
[4] a) E. Guler, C. Kaya, N. Kabay, M. Arda, *Desalination* **2015**, *356*, 85; b) N. Hilal, G. J. Kim, C. Somerfield, *Desalination* **2011**, *273*, 23; c) M. M. Nasef, M. Nallappan, Z. Ujang, *React. Funct. Polym.* **2014**, *85*, 54.
[5] a) S. V. Eaton, *Plant Physiol.* **1940**, *15*, 95; b) C. D. Hunt, *J. Trace Elem. Exp. Med.* **2003**, *16*, 291.
[6] a) D. A. Roe, D. B. Mccormick, R. T. Lin, *J. Pharm. Sci.* **1972**, *61*, 1081; b) F. Xu, H. Goldbach, P. H. Brown, R. W. Bell, T. Fujiwara, C. D. Hunt, S. Goldberg, L. Shi, *Advances in Plant and Animal Boron Nutrition: Proceedings of the 3rd International Symposium on all Aspects of Plant and Animal Boron Nutrition*, Springer, Dordrecht, The Netherlands **2007**.
[7] N. Kabay, E. Guler, M. Bryjak, *Desalination* **2010**, *261*, 212.
[8] a) U. Gemici, G. Tarcan, C. Helvaci, A. M. Somay, *Appl. Geochem.* **2008**, *23*, 2462; b) Q. H. Guo, Y. Zhang, Y. W. Cao, Y. X. Wang, W. D. Yan, *Environ. Sci. Pollut. Res.* **2013**, *20*, 8210; c) M. Korkmaz, B. A. Fil, C. Ozmetin, Y. Yasar, *Bulg. Chem. Commun.* **2014**, *46*, 594; d) S. Sahin, *Desalination* **2002**, *143*, 35.
[9] World Health Organization, *Guidelines for Drinking-Water Quality*, World Health Organization, Geneva, Switzerland **2011**.
[10] a) I. Ali, *Chem. Rev.* **2012**, *112*, 5073; b) I. Ali, V. K. Gupta, *Nat. Protoc.* **2007**, *1*, 2661; c) R. W. Baker, *Membrane Technology and Applications*, Wiley-Blackwell, Oxford, UK **2012**; d) B. Nicolaisen, *Desalination* **2003**, *153*, 355.
[11] L. F. Greenlee, D. F. Lawler, B. D. Freeman, B. Marrot, P. Moulin, *Water Res.* **2009**, *43*, 2317.
[12] a) C. Bellona, J. E. Drewes, P. Xu, G. Amy, *Water Res.* **2004**, *38*, 2795; b) J. R. Werber, A. Deshmukh, M. Elimelech, *Environ. Sci. Technol. Lett.* **2016**, *3*, 112.
[13] E. Guler, D. Ozakdag, M. Arda, M. Yuksel, N. Kabay, *Environ. Geochem. Health* **2010**, *32*, 335.
[14] Y. Xu, J. Q. Jiang, *Ind. Eng. Chem. Res.* **2008**, *47*, 16.
[15] Z. M. Guan, J. F. Lv, P. Bai, X. H. Guo, *Desalination* **2016**, *383*, 29.
[16] a) T. Ben, H. Ren, S. Q. Ma, D. P. Cao, J. H. Lan, X. F. Jing, W. C. Wang, J. Xu, F. Deng, J. M. Simmons, S. L. Qiu, G. S. Zhu, *Angew. Chem., Int. Ed.* **2009**, *48*, 9457; b) N. Chaoui, M. Trunk, R. Dawson, J. Schmidt, A. Thomas, *Chem. Soc. Rev.* **2017**, *46*, 3302; c) S. Qiu, T. Ben, *Porous Polymers: Design, Synthesis and Applications*, Royal Society of Chemistry, Cambridge, UK **2016**.
[17] a) G. Barin, G. W. Peterson, V. Crocella, J. Xu, K. A. Colwell, A. Nandy, J. A. Reimer, S. Bordiga, J. R. Long, *Chem. Sci.* **2017**, *8*, 4399; b) T. Ben, Y. Q. Li, L. K. Zhu, D. L. Zhang, D. P. Cao, Z. H. Xiang, X. D. Yao, S. L. Qiu, *Energy Environ. Sci.* **2012**, *5*, 8370; c) K. Konstas, J. W. Taylor, A. W. Thornton, C. M. Doherty, W. X. Lim, T. J. Bastow, D. F. Kennedy, C. D. Wood, B. J. Cox, J. M. Hill, A. J. Hill, M. R. Hill, *Angew. Chem., Int. Ed.* **2012**, *51*, 6639; d) W. G. Lu, J. P. Sculley, D. Q. Yuan, R. Krishna, Z. W. Wei, H. C. Zhou, *Angew. Chem., Int. Ed.* **2012**, *51*, 7480; e) W. G. Lu, D. Q. Yuan, J. L. Sculley, D. Zhao, R. Krishna, H. C. Zhou, *J. Am. Chem. Soc.* **2011**, *133*, 18126; f) W. G. Lu, D. Q. Yuan, D. Zhao, C. I. Schilling, O. Plietzsch, T. Muller, S. Brase, J. Guenther, J. Blumel, R. Krishna, Z. Li, H. C. Zhou, *Chem. Mater.* **2010**,

22, 5964; g) Y. Yuan, F. X. Sun, H. Ren, X. F. Jing, W. Wang, H. P. Ma, H. J. Zhao, G. S. Zhu, *J. Mater. Chem.* **2011**, *21*, 13498; h) H. Y. Zhao, Z. Jin, H. M. Su, J. L. Zhang, X. D. Yao, H. J. Zhao, G. S. Zhu, *Chem. Commun.* **2013**, *49*, 2780.

[18] a) S. Demir, N. K. Brune, J. F. Van Humbeck, J. A. Mason, T. V. Plakhova, S. A. Wang, G. X. Tian, S. G. Minasian, T. Tyliszczak, T. Yaita, T. Kobayashi, S. N. Kalmykov, H. Shiwaku, D. K. Shuh, J. R. Long, *ACS Cent. Sci.* **2016**, *2*, 253; b) S. Lee, G. Barin, C. M. Ackerman, A. Muchenditsi, J. Xu, J. A. Reimer, S. Lutsenko, J. R. Long, C. J. Chang, *J. Am. Chem. Soc.* **2016**, *138*, 7603; c) Y. Yuan, Y. J. Yang, X. J. Ma, Q. H. Meng, L. L. Wang, S. Zhao, G. S. Zhu, *Adv. Mater.* **2018**, *30*, 1706507; d) B. Y. Li, Y. M. Zhang, D. X. Ma, Z. Shi, S. Q. Ma, *Nat. Commun.* **2014**, *5*, 5537; e) B. Y. Li, Q. Sun, Y. M. Zhang, C. W. Abney, B. Aguila, W. B. Lin, S. Q. Ma, *ACS Appl. Mater. Interfaces* **2017**, *9*, 12511; f) J. Li, X. Dai, L. Zhu, C. Xu, D. Zhang, M. A. Silver, P. Li, L. H. Chen, Y. Z. Li, D. W. Zuo, H. Zhang, C. L. Xiao, J. Chen, J. Diwu, O. K. Farha, T. E. Albrecht-Schmitt, Z. F. Chai, S. A. Wang, *Nat. Commun.* **2018**, *9*, 3007.

[19] E. A. Karakhanov, M. Gotszyun, I. S. Kryazheva, M. Y. Talanova, M. V. Terenina, *Russ. Chem. Bull.* **2017**, *66*, 39.

[20] T. M. Ting, M. M. Nasef, K. Hashim, *RSC Adv.* **2015**, *5*, 37869.

[21] N. Bin Darwish, V. Kochkodan, N. Hilal, *Desalination* **2015**, *370*, 1.

[22] J. F. Lyu, Z. L. Z. Zeng, N. Zhang, H. X. Liu, P. Bai, X. H. Guo, *React. Funct. Polym.* **2017**, *112*, 1.

[23] F. M. Chen, L. Guo, X. M. Zhang, Z. Y. Leong, S. Y. Yang, H. Y. Yang, *Nanoscale* **2017**, *9*, 326.

[24] J. F. Lyu, H. X. Liu, Z. L. Z. Zeng, J. S. Zhang, Z. X. Xiao, P. Bai, X. H. Guo, *Ind. Eng. Chem. Res.* **2017**, *56*, 2565.

[25] a) J. Sanchez, B. L. Rivas, E. Nazar, M. Bryjak, N. Kabay, *J. Appl. Polym. Sci.* **2013**, *129*, 1541; b) L. Wang, T. Qi, Z. Gao, Y. Zhang, J. Chu, *React. Funct. Polym.* **2007**, *67*, 202.

[26] K. Yoshimura, Y. Miyazaki, F. Ota, S. Matsuoka, H. Sakashita, *J. Chem. Soc., Faraday Trans.* **1998**, *94*, 683.

[27] D. Peak, G. W. Luther, D. L. Sparks, *Geochim. Cosmochim. Acta* **2003**, *67*, 2551.

[28] Y. S. Ho, G. McKay, *Process Biochem.* **1999**, *34*, 451.

[29] J. Weber, M. Antonietti, A. Thomas, *Macromolecules* **2008**, *41*, 2880.

[30] H. D. Qian, S. H. Li, J. F. Zheng, S. B. Zhang, *Langmuir* **2012**, *28*, 17803.